Computer Microvision for MEMS

Academic and Research Staff
Professor Dennis M. Freeman, Professor Donald E. Troxel

Research Scientist

Michael B. McIlrath

Research Associates

C. Charles Abnet, Abraham R. McAllister, Michael S. Mermelstein

Post-Doctoral Student

Werner Hemmert

Graduate Students

Michael J. Gordon, Stanley Hong, Jekwan Ryu, Samson Timoner, Ramon Rodriguez, Danny Seth, Xudong Tang

Undergraduate Student

Tim Dunn

Technical and Support Staff

Francis M. Doughty

Sponsors

Defense Advanced Research Projects Agency
Grant F30602-97-2-0106

1 Overview

Microelectromechanical systems (MEMS) are fabricated using batch techniques that are similar to those used to fabricate microelectronic devices. Unlike electronics, however, simple methods for testing and characterizing internal failure modes of micromechanical devices do not exist.

The major goal of this project is to develop inexpensive and reliable tools for *in situ* visualization of the motions of internal structures in MEMS by combining light microscopy, video imaging, and machine vision. Images of microelectromechanical systems are magnified with a microscope and projected onto a CCD camera. Stroboscopic illumination is used to take temporal sequences of images at multiple planes of focus. Recorded images are then viewed at playback speeds chosen to facilitate human interpretation of the motions. Quantitative estimates of motions are also obtained directly from the recorded images using algorithms originally conceived for robot vision.

2 Motion analysis algorithms

We have previously developed a direct, hierarchical method for estimating six degree-of-freedom rigid-body motion from sequences of 3D images. Early studies suggested that the method was quite precise. However, more recent studies showed that results can be very sensitive to analysis parameters, such as the size of the analysis region and the number of stages of spatial decimation in the hierarchy. We have never

seen such problems using our 3D translation algorithms. Therefore, we investigated why rotation estimates may be more difficult than translation estimates.

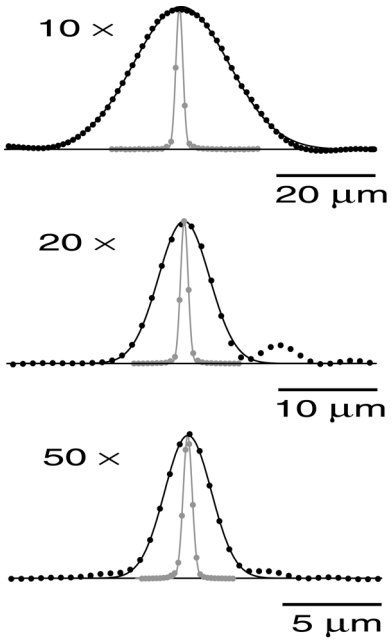

Figure 1: *Measured brightfield point spread functions. A fluorescent polystyrene microsphere (0.5 μm diameter) was imaged with epi-illumination and the resulting 3D fluorescent image was measured. The panels show results for the three objectives we most frequently use for measuring MEMS:*
a Zeiss LD Epiplan-50 × (NA 0.6, working distance 3.5 mm),
a Zeiss LD Epiplan-20 × (NA 0.4, working distance 9.8 mm), and
a Zeiss LD Epiplan-10 × (NA 0.2, working distance 20 mm).
Circles indicate measured brightnesses along lines of symmetry in the axial (black) and transverse (gray) directions. The lines show least-square fits to theoretical diffraction-limited point spread functions (Principles of Optics, Born and Wolf, 1970).

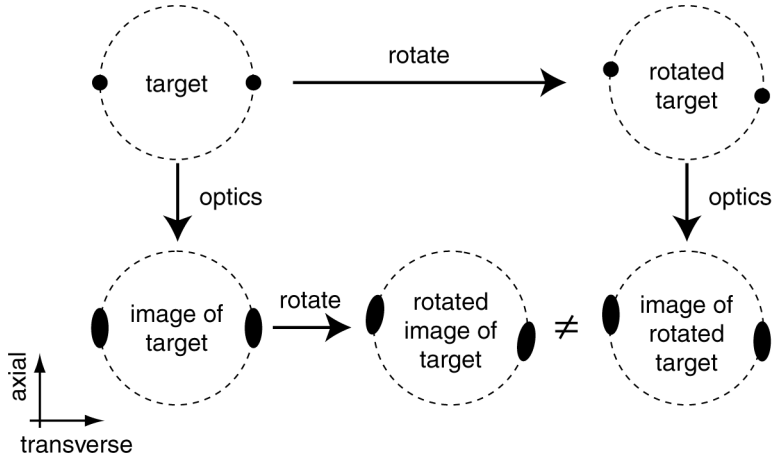

Figure 2: *Effect of anisotropic blurring on rigid-body rotation. A target that consists of two points is shown in the top left sketch. The image of the target is blurred by an anisotropic point spread function (bottom left): there is significantly greater blurring in the axial direction (illustrated vertically) than in the lateral direction. The target is rotated by 10° (top right). The blurred image of the rotated target (bottom right) is not a rigid-*

body rotation of the blurred image of the unrotated target (bottom center). We refer to this effect of anisotropic blurring as the "ferris wheel problem."

One major reason that estimating translations and rotations may differ is that the point spread function of an optical microscope is not isotropic: blurring along the axial direction is significantly greater than blurring within the plane (Figure 1). It follows that rigid-body rotations of a target will not necessarily lead to rigid-body rotations of its image (see Figure 2).

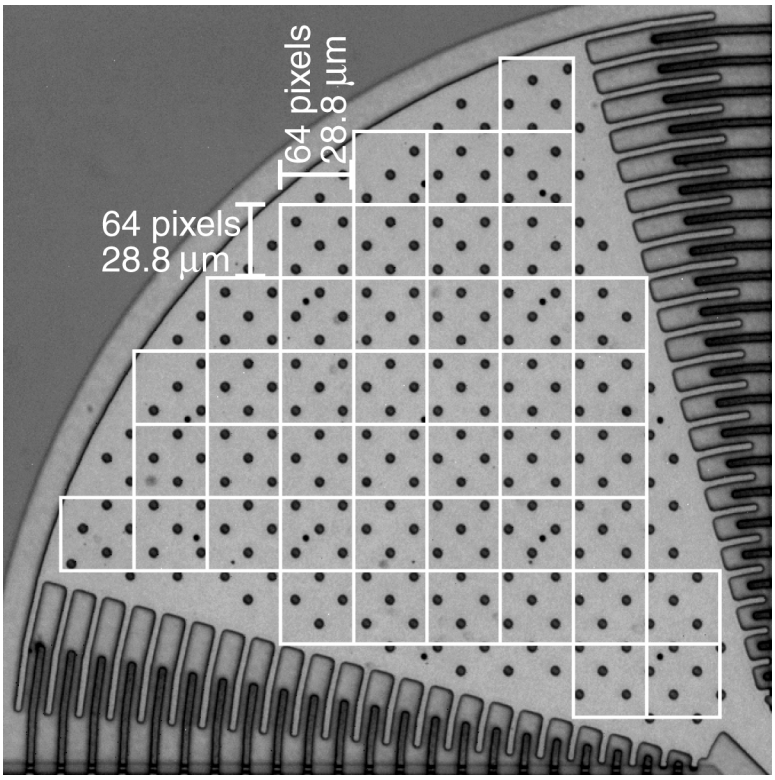

Figure 3: *Estimating rotations from translations. Images are divided into non-overlapping regions. Translations are determined for each region. Rotation of the target is estimated from the set of translations using a least squares procedure.*

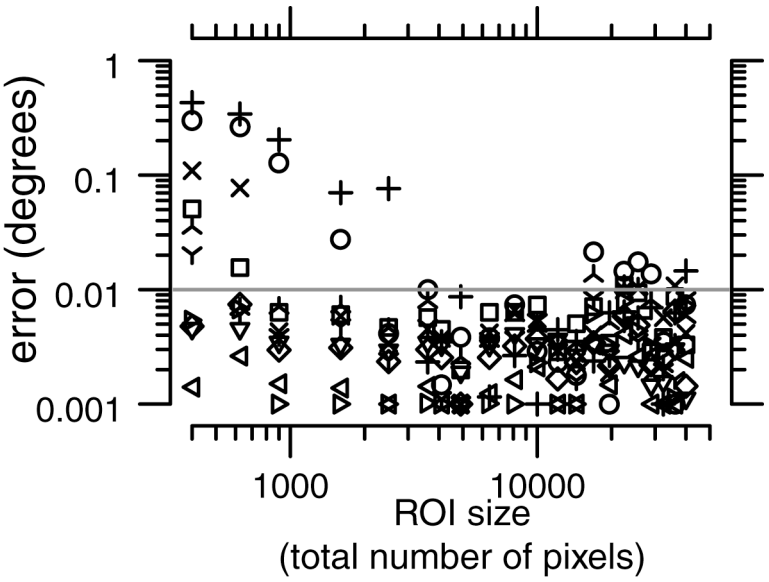

Figure 4: *Dependence of measurement error on size of region of interest. Errors in the angles obtained by least-squares fits to translations of multiple regions are shown for 10 different angular displacements ranging from −1 to +1 degree. Accuracy below 10 millidegrees is attainable using region sizes between 3600 pixels and 14400 pixels (60 to 120 pixels on a side).*

Motivated by Figure 2, we developed an algorithm for estimating rotations from translations. A rigid target is divided into regions as shown in Figure 3. Each region should be small enough so the motion in the region can be approximated as translational. Conversely, the regions should be large enough so that the magnitude of motion is smaller than the dimensions of the region. If the region were too small the image would move completely out of the region from one time increment to the next. There are also statistical considerations in choosing the region size. The available surface area of the target can be divided into many small regions, but results from smaller regions will be more affected by measurement noise. Thus smaller regions lead to more numerous, but more noisy translational estimates than do larger regions. After estimating the translations of each region, rotation of the rigid body is calculated using a least-squares method.

We tested the method by mounting the target to a rotation stage (Newport) that could be rotated with an accuracy of 0.7 millidegrees. Images were acquired at 10 angles ranging from −1 to 1 degree. Images were analyzed by dividing the surface area of the moving shuttle into non-overlapping square regions ranging in size from 20 pixels on a side (400 total pixels) to 200 pixels on a side (40000 total pixels). The absolute differences between the estimated angles and the reference angles are plotted for each region size in Figure 4. There is a range in region sizes from 3600 to 14400 total pixels (60 to 120 pixels on a side) where the absolute errors for all rotation estimates are less than 10 millidegrees.

We suspect that the larger errors for small regions resulted at least in part because the regions were small compared displacements caused by rotation of the stage. One degree of rotation produced motions of the shuttle on the order of 10 pixels. In principle, this source of error can be eliminated by allowing the translational motion estimators to “follow” motions as they move out of one region and into the next. We are currently implementing such algorithms.

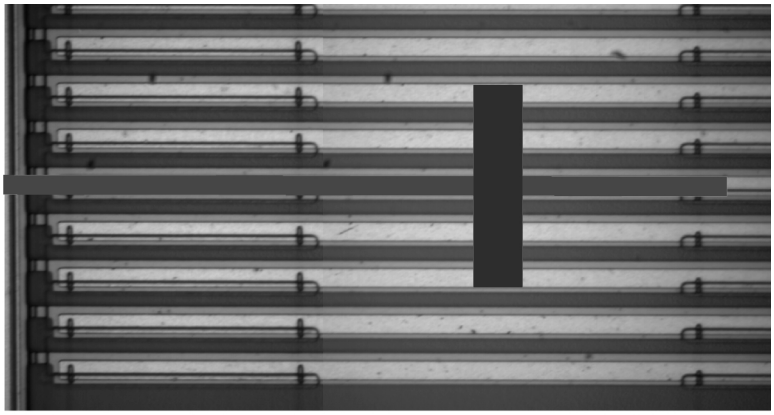

Figure 5: *MEMS optical grating. This brightfield image shows a portion of the optical grating that contains 8 horizontal elements, each of which is brighter than the surrounding substrate. The elements are more than 300 μm long and their centers are 20 μm apart. Voltages can be applied between the elements and the substrate to modulate the out-of-plane distance and tilt of the element. The red and blue bars mark analysis regions. The length of the red bar is 300 μm.*

3 Measuring static deflections of optical gratings using Interferometric Computer Microvision

In collaboration with James Castracane at the University of Albany, we have applied Interferometric Computer Microvision to measure MEMS optical gratings (Figure 5). The gratings consist of an array of slender elements, each approximately 12 μm wide. Our goal was to measure the out-of-plane positions of the elements.

Interferograms were obtained for 3 positions of the reference mirror for each of 7 excitation voltages (DC). Brightnesses in the 3 interferograms were used to determine the optical phase of the interference at each pixel. Phases were "unwrapped" by adding the integral multiple of 2π that minimized first spatial differences.

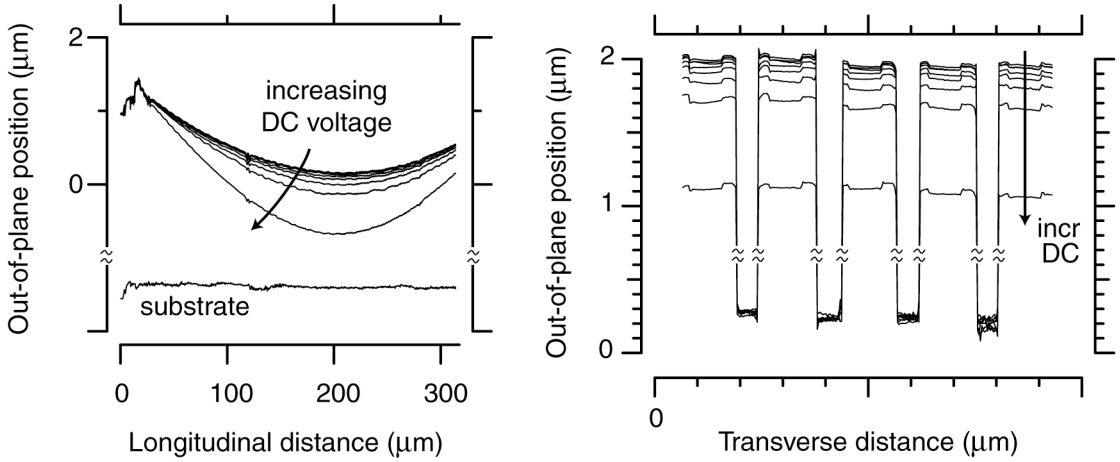

Figure 6: *Out-of-plane positions of grating elements. Curves in the left panel indicate out-of-plane position (ordinate) as a function of distance along the length of a grating element (red line in Figure 5). Each of the upper curves shows results for a different excitation voltage from 0 to 30V in 5V steps. The lower trace shows the out-of-plane position of the substrate lateral to the measured grating element. No attempt was made to determine the number of phase wraps between the element and substrate, as indicated by the broken axis. Curves in the right panel indicate out-of-plane position across the widths of 5 elements (blue line in Figure 5) for the same excitation voltages.*

Results shown in the left panel of Figure 6 illustrate bending of the elements as a function of distance along the long axis of the element. In the absence of DC excitation, the element sags approximately 1 μm across its more than 300 μm length. The bending increases as the applied voltage is increased. Measurements of the adjacent substrate show no similar sagging.

The right panel of Figure 6 shows out-of-plane displacement across 5 adjacent elements. Displacements were obtained for the more than 25 pixels that span the approximately 12 μm width of each element. Although these elements are designed to tilt, little tilt is seen in these measurements.

These results clearly indicate that Interferometric Computer Microvision can be used to assess both out-of-plane position and tilt of MEMS optical gratings.

4 Speckle Heterodyne Microscopy

As part of our effort to develop new optical and imaging methods for measuring motions of MEMS, we have investigated novel imaging schemes that are based on structured laser illumination.

In a typical light microscope, the light source is optically crude, providing approximately uniform illumination to the target. On the other hand, the microscope objective, the first and most critical element in the imaging chain, is optically sophisticated. Therefore, the optical quality of the objective is primarily responsible for the optical quality of the microscope. In *Speckle Heterodyne Microscopy*, we adopt an alternative strategy: coupling highly precise structured illumination from a laser source with a relatively crude detection system. Using laser light with beam-splitting and steering techniques, we can generate precisely structured illumination, such as high-spatial-frequency fringe and speckle patterns. These patterns selectively excite microscopic features of the target. Therefore, the key to resolution in the revised strategy is in the illuminator --- not in the detector. By using finely-patterned laser illumination, we can obtain high resolution images using low resolution optics and a CCD camera.

Pixels in a CCD camera report a single output value that represents the sum of the photons that strike any part of the pixel. By controlling the fine structure of the source of illumination, low resolution pixels become sensitive to high resolution structure in the target. After acquiring a sequence of images with different structured illumination patterns, we can use a computer to post process the images and enhance the resolution of each CCD pixel to the resolution of the illumination patterns.

Experimental verification of theory

We have constructed a series of prototypes, each designed to test practical engineering ideas as well as fundamental science. The experimental verification of speckle heterodyne theory marked the completion of a Ph.D. thesis: *Synthetic Aperture Microscopy*, by Michael Mermelstein, a Hertz Fellow and member of our research group. The thesis reports on the theory of speckle heterodyne microscopes, on engineering practical ones, and on the group's progress with various prototype experimental systems.

One of our prototypes, shown in Figure 7, uses forty-one (41) beams from an argon ion laser operated at 488 nm (blue) to generate finely-structured illumination. The phase of each beam is controlled by a custom 128 channel digital-to-analog converter under computer control. Light reflected from the target is collected by a 256×256 pixel CCD camera with 16 μm pixels and a $2\times$ copy lens.

The Fourier transform of a measured illumination pattern created by the interference of these 41 beams is shown in Figure 8. This measurement contains a pattern of 1,641 bright spots (two for each beam-pair and one at the origin) located in accordance with the theoretically predicted arrangement. The figure demonstrates the prediction that the patterns created by the 41 beams provides an excellent and predictable sampling of Fourier space.

The outer ring of points in the Fourier transform marks the highest spatial frequency that is sampled, which corresponds to a resolution of 0.2 μm (with 0.488 μm illumination!). This corresponds to a factor of 40 increase in the effective resolution of the CCD and lens system. Furthermore, this high resolution is achieved with large working distance (greater than 12 cm) and field of view (greater than 4 mm square).

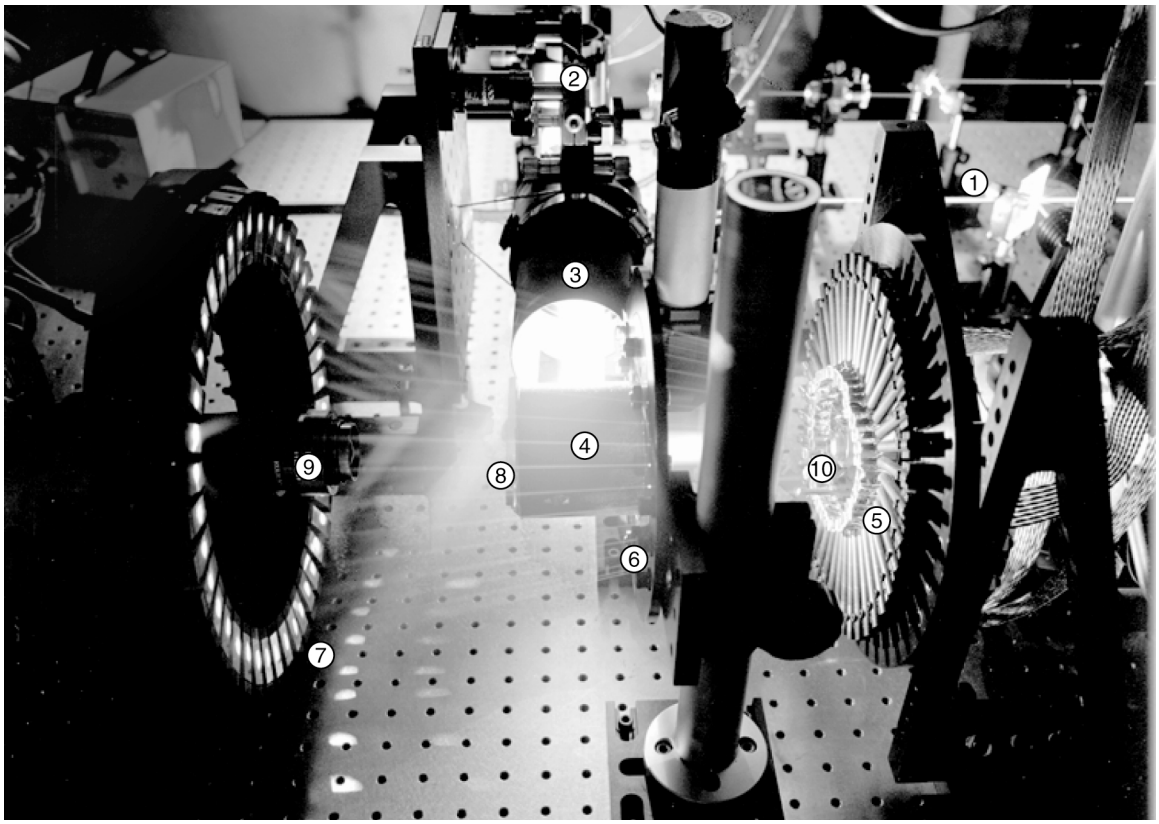

Figure 7: *A speckle heterodyne microscope experimental setup. The labels indicate (1) the source beam from the argon ion laser (laser head not shown) which passes through a spatial filter before entering (2) a periscope assembly which directs the expanding beam into (3) a large aperture copy lens. The now converging beam enters (4) the hologram housing which contains an elliptical fold mirror and the beam-splitting hologram. A diverging cone of 41 converging beams emerges from the right side. The beams strike (5) the ring of path-length modulating mirrors, one beam per mirror. Each mirror is glued to a piezo which is glued to a steel drill-rod post. Each post fastened to a miniature tip-tilt mount to facilitate alignment with (6) the "slit array," an array of matched spatial filters at the unfolded focus point of the copy lens. The now diverging beams strike gratings in (7) the grating wheel from which they diffract. Second-order diffracted beams are the strongest (because of the blaze angle of the gratings), and a converging cone of diverging second-order beams land on (8) the target where they interfere,* ***forming the finely-structured illumination pattern****. Light scattered or fluoresced by the* ***illuminated micro-regions*** *of the target is collected by (9) the target* ***camera macro lens****. First-order diffracted beams from the grating wheel pass through angled cuts in the slit-wheel mounting plate and interfere in the focal plane of (10) the reference camera microscope objective lens for calibration of the phase offsets of the many beams.*

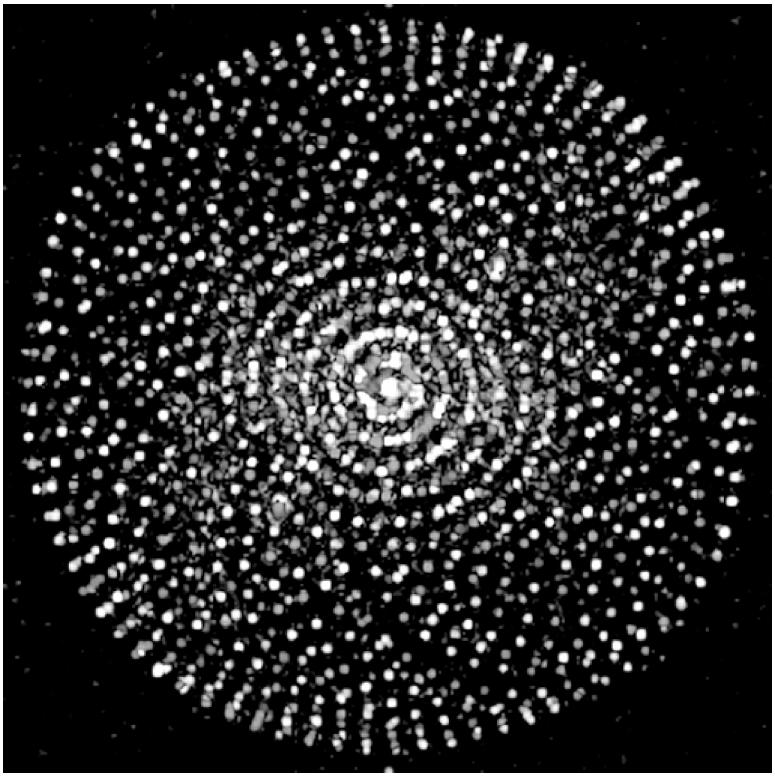

Figure 8: *Processed data from the setup in Figure 7.*

Summary. Speckle Heterodyne Microscopy enables

1. Order-of-magnitude **improvement in depth of field**. This improvement is particularly useful for high-resolution inspection of MEMS systems with substantial depth compared to in-plane detail such as (1) hinged, tilted devices like 90-degree mirrors, (2) high aspect-ratio MEMS, and (3) MEMS interface to packaging feed-throughs. While these systems are currently sufficiently visualized *statically, in a resting state* using scanning electron microscopy (SEM), an optical inspection capability can provide the *dynamic visualization of functioning systems* that is critical to MEMS characterization.
2. Order-of-magnitude **improvements in field of view**, useful for measuring large fields of devices such as large MEMS arrays, and
3. Order-of-magnitude **improvements in working distance**, useful for *in-situ* process monitoring.

5 Computer Microvision for MEMS

Project Staff
Xudong Tang, Danny Seth, Michael B. McIlrath, Donald E. Troxel

MEMS have the potential to revolutionize the design and production of sensors and actuators. However, the ultimate introduction of MEMS into major military and commercial systems depends critically on the speed with which MEMs can be designed and delivered into the field. The paucity of test equipment now available is an obstacle to the dissemination of MEMS for increasing the nation's defense and commercial competitiveness.

We call computer microvision the combination of light microscopy, video imaging, and machine vision. We are developing a series of MEMS stations to collect image data on various MEMS devices. The series of measurement stations will have a modular structure to enable the deployment of cost-effective measurement stations for the task at hand. A relatively more expensive MEMS station will have expanded

specifications. Our ultimate goal is to develop computer microvision as a useful tool for the design and manufacture of MEMS - a tool that will enable the measurement of dynamical properties of the materials used to fabricate the MEMS device, as well as to characterize MEMS components used in larger systems.

Work has proceeded in the construction of a MEMS station consisting of a pc, camera, probe station (including a microscope), stimulus generator, and strobe pulse generator. This system will provided pictures in order to analyze a candidate MEMS device. Considerable work has been done on the development of a strobe pulse generator to trigger a flash tube which illuminates the image to be captured. A novel technique for the generation of these pulses via a software algorithm has been proposed and will be evaluated and compared to the traditional approach using a phase locked loop. We have expanded this goal to include both a memstation which runs pn Windows NT and Linux.

6 Image Sampling Rate Controller: Generating Strobe Pulses in MEM-Station

Project Staff
Ramon L. Rodriguez and Donald E. Troxel

In an effort to support the analysis and development of micro-electromechanical systems, the Research Laboratory of Electronics at the Massachusetts Institute of Technology built a workstation dedicated to testing and troubleshooting MEMS, the MEM-station. When the camera controlled by the MEM-station takes pictures of MEMS under stimulus, specialized hardware in the workstation generates a sequence of pulses that determine the camera's sampling rate. Phase-Locked Loop frequency multipliers provide a solution for the generation of strobe pulses in the MEM-station. The PLL communicates with the workstation using the computer's serial port. The PLL solution allows users to control the frequency multiplication factor, as well as the trigger point of the first pulse with respect to an excitation signal. This PLL solution supports sampling rate frequencies from 1 Hz to 14.1 MHz.

7 Publications

Freeman, D.M., "Computer Microvision for MEMS", invited paper, *Materials Research Society*, Boston, MA, November 30, 1999.

Lee, Z. K., M. B. McIlrath, and D. A. Antoniadis, " Two-Dimensional Doping Profile Characterization of MOSFET's by Inverse Modeling Using I-V Characteristics in the Subthreshold Region," IEEE Transaction on Electron Devices, Vol. 46, No. 8, 1640-1649, (Aug. 1999).

Troxel, D. E., D. S. Boning, and M. B. McIlrath, SSemiconductor Process Representation". Encyclopedia of Electrical and Electronics Engineering, vol. 19, 139-147 (1999).

Theses

Masters Theses

Gordon, M. J., *Rotation analysis of a microfabricated fatique test structure* , MIT Dept. of Electrical Engineering and Computer Science, February, 1999.

Lin, Calvin J. "A New Lab for 6.111: A Coin Operated Vending Machine Controller," M. Eng., Dept. of Electr. Eng.and Comput. Sci., MIT May 1999

Pedersen, Erik J., "User Interface for MEMS Characterization System," M. Eng., Dept. of Electr. Eng.and Comput. Sci., MIT January 1999

Rodriguez, Ramon, "Performance Measurements for MEMS Analysis System," M. Eng., Dept. of Electr. Eng.and Comput. Sci., MIT May 1999

Timoner, S., *Subpixel motion estimation from sequences of video images*, MIT Dept. of Electrical Engineering and Computer Science, June, 1999.

Doctoral Theses

Mermelstein, M. S., *Synthetic Aperture Microscopy*, MIT Dept. of Electrical Engineering and Computer Science, June, 1999.